HHS Public Access

Author manuscript

Adv Funct Mater. Author manuscript; available in PMC 2018 September 13.

Published in final edited form as:

Adv Funct Mater. 2017 September 13; 27(34): . doi:10.1002/adfm.201702928.

Renal-Clearable PEGylated Porphyrin Nanoparticles for Image-guided Photodynamic Cancer Therapy

Dr. Liang Cheng[1,2], **Dr. Dawei Jiang**[2], **Dr. Anyanee Kamkaew**[2,5], **Mr. Hector F. Valdovinos**[3], **Dr. Hyung-Jun Im**[2], **Dr. Liangzhu Feng**[1], **Dr. Christopher G. England**[3], **Ms. Shreya Goel**[4], **Dr. Todd E. Barnhart**[3], **Prof. Zhuang Liu**[1], and **Prof. Weibo Cai**[2,3,4]

[1]Institute of Functional Nano & Soft Materials (FUNSOM), Collaborative Innovation Center of Suzhou Nano Science and Technology, Soochow University, Suzhou, Jiangsu 215123, China [2]Departments of Radiology, University of Wisconsin-Madison, Wisconsin 53705, United States [3]Department of Medical Physics, University of Wisconsin-Madison, Wisconsin 53705, United States [4]Materials Science Program, University of Wisconsin-Madison, Wisconsin 53705, United States [5]School of Chemistry, Institute of Science, Suranaree Institute of Science, Nakhon Ratchasima 30000, Thailand

Graphical Abstract

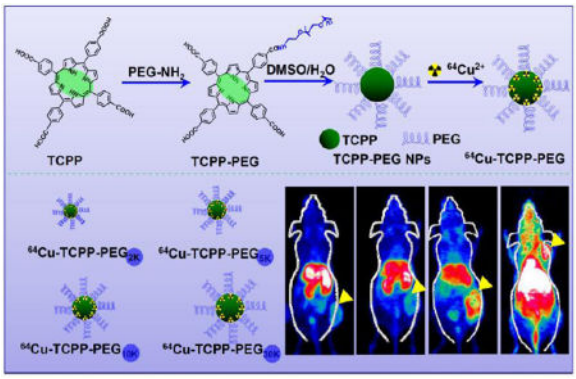

Noninvasive dynamic positron emission tomography (PET) imaging was used to investigate the balance between renal clearance and tumor uptake behaviors of polyethylene glycol (PEG)-modified porphyrin nanoparticles (TCPP-PEG) with various molecular weights. TCPP-PEG_{10K} nanoparticles with clearance behavior would be a good candidate for PET image-guided photodynamic therapy.

Keywords

TCPP-PEG nanoparticles; Renal clearance; Dynamic PET imaging; Fluorescence imaging; Photodynamic therapy

Correspondence to: Liang Cheng; Weibo Cai.

Supporting Information

Supporting Information is available online from the Wiley Online Library or from the author.

Cancer has overtaken heart disease to become the leading cause of death worldwide[1]. Fortunately, with the continued development of nanomaterials and nanotechnology, new types of effective cancer treatment, such as photothermal therapy (PTT) and photodynamic therapy (PDT), have emerged as powerful cancer therapy techniques[2]. Various inorganic/organic nanomaterials including carbon-based nanomaterials, gold-based nanomaterials, metallic nanoparticles, transition metal dichalcogenides, organic polymers, and albumin carriers have shown great potential for cancer treatment due to the unique physiochemical properties[2a, 2b, 3] However, most of these nanoparticles suffer from high uptake by the reticuloendothelial system (RES), resulting in slow and inefficient clearance. According to the U. S. Food and Drug Administration (FDA) principle, any diagnostic or therapeutic agent should be completely cleared from the body within a reasonable period of time[4]. Considering the unique structure of the glomerular capillary wall, only ultra-small nanoparticles with hydrodynamic diameters less than 5.5 nm can pass through the kidneys and rapidly undergo renal excretion. Previous studies have shown that nanoparticles ranging from 15 to 50 nm are readily sequestered by the RES, while those nanoparticles larger than 50 nm undergo partial hepatobiliary clearance[5]. In general, renal clearance is much faster than hepatobiliary clearance. Both nanoparticles size and surface coating will affect the hydrodynamic diameters (HDs) and the way in which the nanoparticle is cleared from the body[5a, 6], and it is a great challenge to fabricate renal clearable nanomaterials.

In clinical applications, increased circulation time and exposure of nanomaterials to healthy tissues has strongly correlated with increased toxicities and adverse effects. However, the rapid removal of nanoparticles by renal clearance results in lower tumor accumulation, weaker imaging sensitivity, and poorer therapeutic effects. Therefore, it is difficult to design nanomaterials that satisfy the balance between the imaging and therapeutic desires and the requirement for renal clearance within a reasonable timescale[4–5, 5f, 7]. Recently, glutathione-coated ultra-small gold nanoparticles (2.3 ± 0.3 nm) showed rapid renal clearance. However, the ultra-small gold nanoparticles displayed slow clearance and gradual passive tumor retention after coating with PEG. Liu *et al.* also developed iron coordination polymer nanodots with renal clearance properties for cancer theranostic applications[8]. Ultra-small polymer nanodots showed excellent renal clearance and effectively accumulated in the tumor via the EPR effect for magnetic resonance imaging-guided PTT. However, fabricating renal clearable nanomaterials with desirable multiple functionalities remains a great challenge.

Herein, we investigate the clearance and tumor uptake behavior of nanoparticles using *meso*-tetra(4-carboxyphenyl)porphyrin (TCPP) fabricated with polyethylene glycol (PEG) as a model. TCPP and their derivatives are widely employed for cancer diagnosis and PDT, as they have shown enhanced affinity to cancer cells. However, the hydrophobic nature of most porphyrins has limited their potential use in clinic. We hypothesize that the addition of PEG to TCPP would enhance the aqueous solubility and increase the molecular volume, resulting in enhanced tumor localization. Thus, different molecular weights of PEG molecule (2K, 5K, 10K, and 30K) are conjugated to TCPP and the resulting TCPP-PEG nanoparticles are tested for clearance and tumor uptake behaviors. Moreover, TCPP is a good chelating agent for the isotope $^{64}Cu^{2+}$, a useful PET radionuclide with a 12.7 h half-life, for PET imaging[9]. As a noninvasive analytical technique, we firstly investigate the dynamic positron emission

tomography (PET) imaging of TCPP-PEG nanoparticles with various molecule weights after intravenous (i. v.) injection. It was found that larger sizes of the nanoparticles are better for tumor uptake, while the smaller ones are more amenable to renal clearance. Under the guidance of PET and fluorescence dual-modality imaging, TCPP-PEG_{10K} nanoparticles with a HD size of ~10 nm would be a good candidate for balancing of clearance and tumor uptake behaviors. *In vitro* and *in vivo* PDT is carried out which gave excellent therapeutic efficacy for the selected nanoparticles. Our study presents a simplified approach to fabricate and indicate biocompatible multifunctional TCPP-PEG-based theranostic agents with clearance behavior, which highlights the clinical application potential of TCPP-PEG nanoparticles as theranostic probes for image-guided cancer therapy.

TCPP porphyrin nanoparticles with various molecular weights of PEG chains were synthesized using a simple amide coupling reaction (Figure 1a). Unlike the previous porphyrin-PEG mesh structure[10], only a single NH_2 terminal of PEG polymer was used. Carboxyl groups on TCPP were first activated with EDC and then PEG was added into the reaction with a ratio of 2 : 1 (TCPP : PEG) to ensure only one carboxyl group of TCPP molecule was conjugated with a single polymer chain of PEG. After the reaction, several suitable filters were used to remove excess free TCPP molecules and coupling reagents. Matrix-assisted desorption/ionization time-of-flight (MALDI-TOF) spectra were used to confirm the molecular weight of the various synthesized TCPP-PEG (2K, 5K, 10K, and 30K) polymers. From the spectra, we found mostly single PEG polymers were linked to the surface of TCPP molecules to form TCPP-PEG nanoparticles with various molecular weights based on the PEG used for synthesis (Supporting Figure S1). However, when the ratios of TCPP : PEG changed to 1:1 or lower, mixtures of TCPP-PEG polymers were found in the system and were too complicated to purify (Supporting Figure S2). ^1H nuclear magnetic resonance (NMR) and Fourier transform infrared (FTIR) spectra also confirmed that various molecular weight of PEG molecules were conjugated on TCPP (Supporting Figure S3 & S4). From the high-performance liquid chromatography (HPLC) spectra, we also found that the retention time was greatly dependent on the molecular weights of the synthesized TCPP-PEG polymers (Supporting Figure S5).Transmission electron microscopy (TEM) images revealed that all these synthesized porphyrin polymers existed in a micelle structure with sizes of 3.6 ± 1.4, 5.4 ± 2.3, 8.8 ± 1.6, and 14.2 ± 2.8 nm for TCPP-PEG_{2K}, TCPP-PEG_{5K}, TCPP-PEG_{10K}, and TCPP-PEG_{30K}, respectively (Figure 1b). By increasing the molecular weight of PEG conjugates, the HDs also increased. The final HDs were 4.6 ± 1.4, 7.5± 2.2, 10.1 ± 2.8, and 17.3 ± 3.2 nm for TCPP-PEG_{2K}, TCPP-PEG_{5K}, TCPP-PEG_{10K}, and TCPP-PEG_{30K} nanoparticles, respectively, agreed with the above TEM results (Figure 1c). All these TCPP-PEG nanoparticles were highly stable in various physiological solutions without aggregation for three months (Supporting Figure S6 & S7). Zeta potential of all TCPP-PEG nanoparticles was slightly negative (Supporting Figure S8) confirming that parts of TCPP-PEG nanoparticles satisfies the size and surface charge threshold requirements for renal clearance. In addition, there was no fluorescence quenching after PEG conjugation (Supporting Figure S9) indicating that our synthesized TCPP-PEG nanoparticles were viable fluorescence imaging agents.

Porphyrins and their derivatives can be readily radiolabeled with copper-64 ($^{64}Cu^{2+}$) for PET imaging, and dynamic PET imaging provides a highly useful tool for studying renal

clearance behavior[11]. By simply mixing $^{64}Cu^{2+}$ with TCPP-PEG nanoparticles at 37 °C for 1 h under constant shaking, we found that $^{64}Cu^{2+}$ was immediately chelated by TCPP-PEG nanoparticles with more than 80% labeling yields for all TCPP-PEG nanoparticles (Figure 2a–2h). Moreover, the ^{64}Cu-labeled TCPP-PEG nanoparticles (^{64}Cu-TCPP-PEG) were also found to be highly stable in serum for 48 h, even in a 1,4,7-triazacyclononane-1,4,7-triacetic acid (NOTA) competitive situation (Figure 2i–2l). Such highly efficient and stable intrinsic radiolabeling radiolabeling of nanoparticles would be suitable for *in vivo* PET imaging. In order to investigate both clearance and tumor uptake behaviors, we used BALB/c mice bearing murine breast cancer 4T1 tumors. Mice were intravenously (i. v.) injected with ~10 MBq of various ^{64}Cu-TCPP-PEG nanoparticles (2K, 5K, 10K, and 30K) and imaged by a microPET/microCT Inveon rodent model scanner. Figure 3a shows the representative maximum intensity projections (MIPs) of coronal PET images depicting the *in vivo* biodistribution of ^{64}Cu-TCPP-PEG nanoparticles at 10 s, 1 min, 5 min, 15 min, 30 min, 2 h, 4 h, 6 h, 12 h, and 24 h post-injection (p. i.). During the initial 30 min, a dynamic scan was performed (Supporting Figure S10–S13). Static PET imaging of the same mice was performed to provide more detailed information regarding the clearance of TCPP-PEG nanoparticles at later time points. It was found that all the TCPP-PEG nanoparticles showed high accumulation in the blood pool directly after injection, yet TCPP-PEG nanoparticles were rapidly filtered through kidneys and accrued in the bladder. Interestingly, the blood circulation and metabolic rate showed significant differences among TCPP-PEG nanoparticles with various molecular weights. Figure 3b shows the detailed blood circulation curves of ^{64}Cu-TCPP-PEG nanoparticles during the initial 4 h. Classical two-compartment pharmacokinetics were observed for all the TCPP-PEG nanoparticles (Supporting Figure S14a–S14d), with distribution half-life ($t_{1/2\alpha}$) and elimination half-life ($t_{1/2\beta}$) values of 4.26 ± 1.95 min and 10.67 ± 2.15 min for TCPP-PEG_{2K}, 10.84 ± 0.35 min and 28.15 ± 3.55 min for TCPP-PEG_{5K}, 17.62 ± 3.34 min and 40.05 ± 8.70 min for TCPP-PEG_{10K}, 26.83 ± 3.92 min, and 86.9 ± 18.36 min for TCPP-PEG_{30K}, respectively. The $t_{1/2\beta}$ of TCPP-PEG_{30K} nanoparticles was 8.1 times longer than that of TCPP-PEG_{2K} nanoparticles. In addition, the area under the curve (AUC) for TCPP-PEG_{30K} (1082.3 %ID h/g) was 2.6 times larger than that of TCPP-PEG_{2K} (412.2 %ID h/g) at 4 h p. i. (Supporting Figure S14e). The elevated tumor uptake for TCPP-PEG_{30k} was attributed to the enhanced blood circulation. The tumor-targeting efficiencies of the TCPP-PEG_{30K} were determined to be 5.6 ± 1.5 and 6.9 ± 1.1 %ID/g at 4 h and 24 h p. i., respectively, slightly higher than TCPP-PEG_{10K} (4.2 ± 0.7 and 4.7 ± 0.35 %ID/g), but much higher than TCPP-PEG_{2K} (2.3 ± 0.57 and 2.2 ± 0.50 %ID/g) and TCPP-PEG_{5K} (2.4 ± 0.57 and 2.8 ± 0.48 %ID/g) nanoparticles (Figure 3c). Such an efficient passive tumor homing of the nanoparticles could be attributed to the enhanced permeability and retention (EPR) effect of 4T1 tumors through the long blood circulation[12].

Next, we carefully investigated the clearance behaviors of these various TCPP-PEG nanoparticles. For TCPP-PEG_{30K} nanoparticles, only radioactive signal in the bladder in the first 30 min was observed. However, strong PET signals were found in the kidneys and bladder in the initial 6 h time point for the lower molecular weight of TCPP-PEG nanoparticles (2K, 5K, and 10K) after i. v. injection, (Figure 3a, Supporting Figure S15a), proving that the majority of them underwent clearance. However, their rate of kidney

filtration varied between the nanoparticles. Detailed biodistribution of ^{64}Cu-TCPP-PEG nanoparticles in the left kidney and bladder were summarized in Supporting Figure S15b & 15c. In the initial 4 h, all the TCPP-PEG nanoparticles showed high signal in bladder with up to 172.1 ± 32.4 %ID/g, except TCPP-PEG$_{30K}$ nanoparticles (9.7 ± 1.4 %ID/g). All the samples showed high signal in the kidneys in the initial time points, indicating that our synthesized TCPP-PEG nanoparticles with small HD sizes can pass through the kidneys for rapid clearance. As expected, the radioactive signal of ^{64}Cu-TCPP-PEG in the kidneys with lower molecular weights (2K and 5K) was stronger than that with larger molecular weights (for example, 10K and 30K) at all time points. In order to investigate the renal-clearable TCPP-PEG nanoparticles, a unilateral ureteral obstruction (UUO) mouse model was used, which was generated by complete ligation of the left ureter of the mouse while the right ureter was kept intact[13] (Supporting Figure S16). After *i.v.* injection of the ^{64}Cu-TCPP-PEG$_{2K}$ nanoparticles, the obstructed left kidney exhibited dramatically reduced radioactivity signals compared to the contralateral right kidney (RK) in UUO mice in the first half an hour, but much higher than the RK at 1 h and 2 h time points post injection. Such a diminished accumulation of contrast agent in the UUO kidney indicated that the blood perfusion had been dramatically reduced upon obstruction, which was consistent with previous findings obtained by SPECT imaging of the UUO mice[14]. Importantly, these finding suggested that glomerular filtration was likely a major clearance route for the small size of nanoparticles, such as TCPP-PEG$_{2K}$ nanoparticles.

The mouse liver also showed the same phenomenon that signal of radioactivity after i. v. injection of TCPP-PEG nanoparticles with the molecular weight less than 10K decreased with the increasing time (Figure 3d, Supporting Figure S17).Uptakes in the liver were 7.2 ± 1.4 %ID/g for TCPP-PEG$_{2K}$, 7.3 ± 1.1 %ID/g for TCPP-PEG$_{5K}$, and 8.8 ± 1.98 %ID/g for TCPP-PEG$_{10K}$ at 24h time point p. i.. Despite high tumor uptake for TCPP-PEG$_{30K}$ nanoparticles, most of them were still deposited in the liver for a long time (up to 17.8 ± 1.6 %ID/g), which was two-times higher than any other smaller molecular weight of TCPP-PEG nanoparticles. Finally, the ^{64}Cu radionuclide dose left in the body was found to be 20.5, 24.2, 28.5, and 50.8 %ID for TCPP-PEG$_{2K}$, TCPP-PEG$_{5K}$, TCPP-PEG$_{10K}$, and TCPP-PEG$_{30K}$ nanoparticles 24 h after i.v. injection of ^{64}Cu-TCPP-PEG nanoparticles (Supporting Figure S18). Considering the balance of clearance and tumor uptake, TCPP-PEG$_{10K}$ nanoparticles were chosen for the following investigation.

In vivo fluorescence imaging conducted at different time points after i. v. injection of TCPP-PEG$_{10K}$ nanoparticles (1 mg/mL, 200 μL) allowed us to further investigate the behaviors of clearance and tumor uptake (Figure 4a, **Supine position**). The TCPP-PEG$_{10K}$ nanoparticles were rapidly excreted into the bladder, and the fluorescence intensity of the bladder area reached its maximum in the initial half hour p. i.. In the remaining time points, we still found strong signal in the bladder, further confirming that TCPP-PEG$_{10K}$ nanoparticles were clearable after i. v. injection. The fluorescence signal from the TCPP-PEG$_{10K}$ nanoparticles also increased in the tumor over time, with the prominent uptake at 24h p.i. (Figure 4a, **Prone position**, Supporting Figure S19), which was consistent with the above PET imaging results. *Ex vivo* imaging at 24h post-injection revealed that TCPP primarily accumulated in the tumor, liver, spleen, and kidneys (Figure 4b, Supporting Figure S20). To further confirm

the tumor accumulation of TCPP-PEG_{10K} nanoparticles, tumor tissues were sectioned and imaged by confocal microscopy. As shown in Figure 4c, strong red fluorescence was clearly visualized in tumor slices, verifying the prominent uptake of TCPP-PEG_{10K} nanoparticles in the tumor, while no fluorescence signal was detected from the tumor tissues devoid of TCPP-PEG_{10K} nanoparticles when using the same imaging condition. The results clearly indicated the efficient tumor passive uptake of our TCPP-PEG_{10K} nanoparticles. Next, we examined the potential toxicities associated with the renal clearance of our nanoparticles. The kidneys were sectioned and investigated for the nanoparticle uptake and cellular toxicity. Strong fluorescence signal was observed from the kidney tissues after 24 h p. i. (Figure 4c), indicating that the nanoparticles passed through the kidneys for clearance. Moreover, the tissues were devoid of any noticeable abnormalities or lesions, confirming the non-toxicity of our TCPP-PEG_{10K} nanoparticles with clearance behavior (Supporting Figure S21).

TCPP porphyrins have been widely used as a photosensitizer for photodynamic cancer therapy and could effectively generate singlet oxygen under light irradiation[15]. It motivated us to investigate the PDT effect of TCPP-PEG_{10K} nanoparticles. Compared with free TCPP, TCPP-PEG_{10K} nanoparticles showed a slightly higher efficiency of light-triggered singlet oxygen production at the same TCPP concentrations (Supporting Figure S22), which was attributed to the better solubility after modification, indicating that the synthesized TCPP-PEG_{10K} nanoparticles could be a better agent for PDT. No significant cytotoxicity was observed for all TCPP-PEG nanoparticles, even at high concentrations of up to 20 μM (Supporting Figure S23). The intracellular uptake of our TCPP-PEG_{10K} nanoparticles was also time-dependent (Supporting Figure S24). Next, we used TCPP-PEG_{10K} nanoparticles as a photodynamic agent for *in vitro* cancer therapy under laser irradiation. The majority of 4T1 cells were destroyed after incubation with 5 μM of TCPP-PEG_{10K} nanoparticles and exposure to the 658 nm laser (Supporting Figure S25a). The PDT effects of TCPP-PEG_{10K} nanoparticles on 4T1 cells were further investigated using Trypan blue staining. Upon laser irradiation, most cells incubated with TCPP-PEG_{10K} nanoparticles were damaged, as indicated by the intense homogeneous blue color (Supporting Figure S25b). The amount of cell death gradually increased upon increasing the concentrations of TCPP-PEG_{10K} nanoparticles. These findings altogether revealed that TCPP-PEG_{10K} nanoparticles hold great promise as an effective photodynamic agent for *in vivo* tumor therapy.

Encouraged by the high PDT efficiency *in vitro* and the efficient passive tumor targeting of TCPP-PEG_{10K} nanoparticles, *in vivo* PDT studies were performed to evaluate the anticancer efficacy of TCPP-PEG_{10K} nanoparticles. For the PDT group (n = 4), the mice were intravenously injected with TCPP-PEG_{10K} nanoparticles (200 μL, 1 mg/mL) and then irradiated for 30 min with the 658-nm laser at 50 mW/cm^2 after 24 h p. i.. As illustrated in Figure 5a, TCPP-PEG_{10K} nanoparticles-mediated PDT can significantly inhibit tumor growth, whereas laser irradiation alone or PBS injection with laser irradiation did not affect the tumor growth. These results suggest that TCPP-PEG_{10K} nanoparticles are a powerful agent for *in vivo* PDT of cancer (Figure 5b). To further understand the PDT effects after various treatments down to the cellular level, hematoxylin and eosin (H&E) staining was utilized to study the morphology and apoptosis of tumor cells after two days post-treatment. The results indicated that most cancer cells were completely destroyed in the TCPP-PEG_{10K}

nanoparticles with laser treatment group (Figure 5c), while cells in the other three control groups mainly retained their normal morphology, further confirming the efficacy of TCPP-PEG_{10K} polymer for *in vivo* photodynamic ablation of cancer.

In summary, our study introduced a simple method to synthesize PEGylated TCPP porphyrin nanoparticles and employed noninvasive dynamic PET imaging to investigate the balance of the renal clearance and tumor uptake behaviors. We found that PEG with larger molecular weights was better for tumor uptake and the lower ones were suitable for renal clearance. Considering this balance, TCPP-PEG_{10K} nanoparticles were the most suitable model to investigate clearance and tumor uptake. *In vitro* and *in vivo* PDT experiments were carried out which led to excellent therapeutic efficacy. Therefore, our work presented a simply fabrication method for selection of biocompatible multifunctional TCPP-PEG-based theranostic agents with renal clearance behavior, which highlights the clinical application potential of TCPP-PEG as theranostic probes for imaging-guided cancer therapy.

Experimental section

Materials

Meso-tetra(4-carboxyphenyl)porphyrin (mTCPP) and Dimethyl sulfoxide (DMSO) were obtained from Frontier Scientific, Inc. (Logan, UT, USA). Polyethylene glycol $(PEG)_{2K}$, PEG_{5K}, PEG_{10K}, and PEG_{30K} were obtained from Biomatrik Co., Ltd. (Jiaxing, China) with the molecular weight of 2 kDa, 5 kDa, 10 kDa, and 30 kDa, respectively. 1-ethyl-3-(3-(dimethylamino)-propyl)carbodimide (EDC), and N-hydroxysulfosuccinimide (Sulfo-NHS) were obtained from Sigma-Aldrich. Deionized water used in our experiments was obtained from a Milli-Q water system.

Synthesis of TCPP-PEG nanoparticles

TCPP-PEG nanoparticles with various molecular weights were synthesized according to the protocol reported previously with slight modification[10]. Firstly, 10 μmol of TCPP was mixed with 5 μmol of EDC and 5 μmol of Sulfo-NHS in 100 μL anhydrous DMSO for 0.5 h at room temperature. Then, PEG with different molecular weight (2K, 5K, 10K, and 30K) in 2 mL water was slowly added to the above-activated TCPP molecules. The molar ratio of PEG-NH_2: TCPP: EDC: NHS was 1: 2: 1: 1. After reacting for 24 h at room temperature, excess TCPP molecules, catalysts, and DMSO were removed by millipore filters with different molecular weight cut off. Afterwards TCPP-PEG_{2K}, TCPP-PEG_{5K}, TCPP-PEG_{10K}, and TCPP-PEG_{30K} nanoparticles in water were obtained and stored at −4 °C for future use. The concentration of TCPP-PEG nanoparticles was defined by TCPP content.

Characterization

Transmission electron microscopy (TEM) images of the nanoparticles were obtained using an FEI Tecnai F30 transmission electron microscope at an acceleration voltage of 300 kV. UV-vis-NIR spectra were obtained with PerkinElmer Lambda 750 UV-vis-NIR spectrophotometer. Fluorescence spectra of different samples were obtained on a FluoroMax 4 luminescence spectrometer (HORIBA Jobin Yvon). The hydrodynamic diameters of TCPP-PEG nanoparticles were determined by a ZetaSizer Nano-ZS (Malvern Instruments,

UK). Matrix-assisted desorption/ionization time-of-flight (MALDI-TOF) spectra of TCPP-PEG nanoparticles were obtained from MDS SCIEX 4800 MALDI TOF/TOF (Applied Biosystems, Foster City, CA, USA). ^{1}H NMR spectra were recorded on a 400 MHz NMR spectrometer (INOVA-400) at 25 °C with $CDCl_3$ as the solvent and tetramethylsilane (TMS) as the internal standard. Fourier transform infrared (FTIR) absorption spectra of the nanoparticles were recorded by using a Nicolet 6700 spectrometer at 4 cm^{-1} resolution, over the wavenumber range 400–4000 cm^{-1}.

Tumor models

All animal studies were conducted under a protocol approved by the University of Wisconsin Institutional Animal Care and Use Committee (IACUC). The 4T1 subcutaneous xenografts were generated by subcutaneous injection of 1×10^6 cells in ~50 μL RMPI-1640 medium onto the back of each female BALB/c mice. In order to investigate the optical imaging of TCPP-PEG nanoparticles, female nude mice were employed. To develop the tumor model, 1×10^6 4T1 cells in ~50 μL PBS were injected onto the back of female nude mice. The mice were used when tumor volumes reached about ~150 mm^3.

^{64}Cu labeling and animal model for dynamic PET imaging

$^{64}Cu^{2+}$ was produced with an onsite cyclotron (GE PET trace). Briefly, $^{64}CuCl_2$ (~150 MBq) was diluted in 300 μL of 0.1 M sodium acetate buffer (pH 5.5) and mixed with 100 μL various kinds of TCPP-PEG nanoparticles (0.1 mg/mL). The reaction was conducted at 37 °C for 1 h with constant shaking. The labeling yield was determined by thin-layer chromatography (TLC) at different time points. The resulting ^{64}Cu-TCPP-PEG (2K, 5K, 10K, and 30K) nanoparticles were purified using PD-10 columns with PBS as the mobile phase.

The serum stability study was carried out to ensure $^{64}Cu^{2+}$ was stably attached on TCPP-PEG nanoparticles. ^{64}Cu-TCPP-PEG nanoparticles with various molecule weights were incubated in complete serum at 37 °C for up to 48 h. At different time points, portions of the mixture were sampled and filtered through MWCO filters with different molecule weights. The retained (i.e., intact) $^{64}Cu^{2+}$ on ^{64}Cu-TCPP-PEG nanoparticles was calculated using the equation (radioactivity on filter/total sampled radioactivity × 100%).

In order to investigate the serum stability of nanoparticles, we not only investigate the stability in mouse serum containing warm media (37 °C), but also added 1,4,7-triazacyclononane-1,4,7-triacetic acid (NOTA) as the stronger challenge chelator to remove unstable ^{64}Cu-labeled TCPP-PEG nanoparticles. 20 μL of NOTA with the concentration of 1 mM was added into 250 μL of ^{64}Cu-TCPP-PEG (~300 μCi) in complete mouse serum solution (pH 7) at 37 °C under constant shaking (~600 rpm) for 48 h. At each time point, 25 μL of the mixture was taken out and re-suspended in 100 μL of NaOAc buffer. A filter was used to separate potential ^{64}Cu-NOTA from ^{64}Cu-TCPP-PEG nanoparticles. The ^{64}Cu-NOTA and ^{64}Cu-TCPP-PEG nanoparticles radioactivity was measured by using a gamma counter (PerkinElmer). ^{64}Cu-TCPP-PEG with various molecule weights was found to be highly stable in warm mouse serum for up to 48 h even with NOTA challenge.

In vivo PET imaging studies were performed in a microPET/microCT Inveon rodent model scanner (Siemens Medical Solutions USA, Inc.) For dynamic PET studies, BALB/c mice planted with 4T1 tumors were anesthetized under isoflurane and their tail vein catheterized. Following this, animals were put in the scanner in a prone position and simultaneously with the injection of ~300 μCi of various kinds of TCPP-PEG nanoparticles (^{64}Cu-TCPP$_{2K}$, ^{64}Cu-TCPP$_{5K}$, ^{64}Cu-TCPP$_{10K}$, and ^{64}Cu-TCPP$_{30K}$), a 30 min emission scan was acquired. List mode files were framed into 28 frames: 6×10 s, 6×30 s, 6 × 60 s, and 10 ×120 s. Another five additional static PET scans at 2 h, 4 h 6 h, 12 h, and 24 h p. i. of the nanoparticles were acquired. Data acquisition, image reconstruction, and ROI analysis of the PET data were performed as described previously[16]. After the PET scans at 24 h, *ex vivo* biodistribution studies were carried out to ensure the %ID/g values determined by PET imaging truly represented the radioactivity distribution in tumor-bearing mice. Mice were euthanized, and blood, tumor, and major organs/tissues were collected and wet-weighed. The radioactivity in the tissue was measured using a gamma-counter (PerkinElmer, USA) and presented as %ID/g (mean ±SD).

Unilateral ureteral obstruction (UUO) model

Mice were anesthetized with 2% isoflurane and the left kidney was exposed through the site of the incision. The ureter was obstructed completely near the renal pelvis using a 4-0 silk tie suture at two points. After two days, *in vivo* dynamic PET imaging studies were performed in a microPET/microCT Inveon rodent model scanner after *i.v.* injection of ~300 μCi of ^{64}Cu-TCPP-PEG$_{2K}$ nanoparticles at various time points. Data acquisition, image reconstruction, and ROI analysis of the PET data were performed as described above.

In vivo fluorescence imaging of TCPP-PEG$_{10K}$ nanoparticles

For *in vivo* imaging, 200 μL of TCPP-PEG$_{10K}$ nanoparticles (1 mg/mL) was intravenously injected into each mouse. *In vivo* fluorescence imaging was conducted using an IVIS Spectrum fluorescence imager. Mice were imaged using a 675 nm/740 nm excitation/ emission filter pair under automatic exposure settings, and fluorescence signal was displayed as radiant efficiency. The mice were sacrificed at 24 h after i. v. injection, with their major organs including the tumor, liver, heart, lung, spleen, and kidneys collected for *ex vivo* imaging. Lastly, the tumor and kidney tissues were frozen in optimum cutting temperature (OCT) solution (SACURA, USA) medium and cut into 8 μm slices for confocal imaging.

Single oxygen detection

The method for singlet oxygen detection was based on the protocol reported previously[17]. In brief, 100 mg of Singlet oxygen sensor green or SOSG (Molecular Probes, USA) was dissolved in 330 mL of methanol to obtain the stock solution of SOSG (0.5 mM). Then, 10 μL of SOSG was added to 2 mL of TCPP-PEG$_{10K}$ nanoparticles solution containing 0.2 mg TCPP. Next, the sample was irradiated by a 658 nm laser at a power density of 20 mW/cm^2. The same concentration of free TCPP molecules dissolved in DMSO/water under laser irradiation was used as the control. The fluorescence intensity of SOSG was measured with an excitation wavelength of 494 nm.

Cell culture experiment

Murine breast cancer 4T1 cells were obtained from American Type Culture Collection (ATCC) and cultured at 37 °C under 5% CO_2. All cell culture related reagents were purchased from Invitrogen. 4T1 cells were cultured in normal RPMI-1640 medium containing 10% fetal bovine serum (FBS) and 1% penicillin/streptomycin. Cells were seeded into 96-well plates at a density of 1×10^4 cells per well and incubated with different concentrations of TCPP-PEG_{10K} nanoparticles for 24 h. Relative cell viabilities were determined by the standard methyl thiazolyl tetrazolium (MTT) assay.

To examine the cellular uptake of TCPP-PEG_{10K} nanoparticles, 4T1 cells were plated in 35 mm dish with 14 mm bottom well (1×10^5 cells per well) for 24 h. After adhesion, TCPP-PEG_{10K} nanoparticles were added into the wells at the concentration of 5 μM (TCPP) and cultured for different time periods (1h, 3 h, 6 h, and 24 h). After washing three times with PBS (pH = 7.4), cells were fixed by 4% paraformaldehyde and labeled with 4', 6-diamidino-2-phenylindole (DAPI) before imaging with a Nikon A1RS confocal microscope and imaging analysis was performed using the NIS-Elements Ar with Deconvolution package.

In vitro photodynamic therapy

For *in vitro* PDT, 4T1 cells (1×10^4) were seeded in 96-well plates and added with TCPP-PEG_{10K} nanoparticles at various concentrations. After incubation for 12 h, the experimental groups were exposed to 658 nm laser irradiation under a power density of 20 mW/cm^2 for 15 min, while the control groups were still cultured in dark. Afterward, all samples were incubated in the dark for another 12 h. In order to determine relative cell viabilities after various treatments, the MTT assay was carried out following the standard protocol. After laser irradiation, cells were washed with PBS and stained with 0.4% Trypan blue (Sigma-Aldrich) before imaged by a Nikon Elipse Ti microscope.

In vivo PDT

To develop the tumor model, 4T1 cells (1×10^6) suspended in 50 μL of PBS were subcutaneously injected into the back of each BALB/c mouse. After the tumor volume reached ~150 mm^3, mice were randomly divided into four groups (n = 4 per group) for various treatments: (i) Control; (ii) Laser only; (iii) TCPP-PEG_{10K} nanoparticles i. v. injection; and TCPP-PEG_{10K} nanoparticles i. v. injection + Laser. TCPP-PEG_{10K} nanoparticles, at a dose of 10 mg/kg, were i. v. injected into mice bearing 4T1 tumors. PDT treatments were conducted 24 h later, with the 658-nm laser at the power density of 50 mW/cm^2 for 30 min. The tumor sizes were measured by a caliper every other day and calculated as the volume = (tumor length) × $(\text{tumor width})^2/2$. Relative tumor volumes were calculated as V/V_0 (V_0 was the initial tumor volume). Two days after treatment, the tumors in each group were dissected to make paraffin sections for further hematoxylin and eosin (H&E) staining.

Supplementary Material

Refer to Web version on PubMed Central for supplementary material.

Acknowledgments

This work was partially supported by the National Research Programs from Ministry of Science and Technology (MOST) of China (2016YFA0201200), the National Natural Science Foundation of China (51572180, 51525203, 51302180), the Post-doctoral science foundation of China (2013M531400, 2014T70542). This work was also partly supported by the University of Wisconsin-Madison, the National Institutes of Health (NIBIB/NCI 1R01CA169365, P30CA014520, T32CA009206, and 1R01EB021336), and the American Cancer Society (125246-RSG-13-099-01-CCE).

References

1. a Holohan C, Van Schaeybroeck S, Longley DB, Johnston PG. Nat. Rev. Cancer. 2013; 13:714–726. [PubMed: 24060863] b Siegel RL, Miller KD, Jemal A. CA: A Cancer Journal for Clinicians. 2015; 65:5–29. [PubMed: 25559415]
2. a Cheng L, Wang C, Feng L, Yang K, Liu Z. Chem. Rev. 2014; 114:10869–10939. [PubMed: 25260098] b Huang X, El-Sayed IH, Qian W, El-Sayed MA. J. Am. Chem. Soc. 2006; 128:2115–2120. [PubMed: 16464114] c O'Neal DP, Hirsch LR, Halas NJ, Payne JD, West JL. Cancer Lett. 2004; 209:171–176. [PubMed: 15159019] d Dolmans DE, Fukumura D, Jain RK. Nat. Rev. Cancer. 2003; 3:380–387. [PubMed: 12724736] e Lovell JF, Liu TW, Chen J, Zheng G. Chem. Rev. 2010; 110:2839–2857. [PubMed: 20104890]
3. a Ng KK, Zheng G. Chem. Rev. 2015; 115:11012–11042. [PubMed: 26244706] b Lucky SS, Soo KC, Zhang Y. Chem. Rev. 2015; 115:1990–2042. [PubMed: 25602130] c Lee D-E, Koo H, Sun I-C, Ryu JH, Kim K, Kwon IC. Chem. Soc. Rev. 2012; 41:2656–2672. [PubMed: 22189429] d Kamkaew A, Lim SH, Lee HB, Kiew LV, Chung LY, Burgess K. Chem. Soc. Rev. 2013; 42:77–88. [PubMed: 23014776] e Gao D, Gao L, Zhang C, Liu H, Jia B, Zhu Z, Wang F, Liu Z. Biomaterials. 2015; 53:229–238. [PubMed: 25890722] f Qian C, Yu J, Chen Y, Hu Q, Xiao X, Sun W, Wang C, Feng P, Shen Q-D, Gu Z. Adv. Mater. 2016; 28:3313–3320. [PubMed: 26948067] g Sheng Z, Hu D, Zheng M, Zhao P, Liu H, Gao D, Gong P, Gao G, Zhang P, Ma Y. ACS Nano. 2014; 8:12310–12322. [PubMed: 25454579] h Cheng L, Liu J, Gu X, Gong H, Shi X, Liu T, Wang C, Wang X, Liu G, Xing H. Adv. Mater. 2014; 26:1886–1893. [PubMed: 24375758]
4. Choi HS, Frangioni JV. Mol. Imaging. 2010; 9:291–310. [PubMed: 21084027]
5. a Soo Choi H, Liu W, Misra P, Tanaka E, Zimmer JP, Itty Ipe B, Bawendi MG, Frangioni JV. Nat. Biotechnol. 2007; 25:1165–1170. [PubMed: 17891134] b Zhou C, Long M, Qin Y, Sun X, Zheng J. Angew. Chem. Int. Ed. 2011; 50:3168–3172.c Choi CHJ, Zuckerman JE, Webster P, Davis ME. Proc. Natl. Acad. Sci. 2011; 108:6656–6661. [PubMed: 21464325] d Zhang X-D, Chen J, Min Y, Park GB, Shen X, Song S-S, Sun Y-M, Wang H, Long W, Xie J, Gao K, Zhang L, Fan S, Fan F, Jeong U. Adv. Funct. Mater. 2014; 24:1718–1729.e Liu J, Wang P, Zhang X, Wang L, Wang D, Gu Z, Tang J, Guo M, Cao M, Zhou H, Liu Y, Chen C. ACS Nano. 2016; 10:4587–4598. [PubMed: 27014806] f; g Liu J, Yu M, Zhou C, Yang S, Ning X, Zheng J. J. Am. Chem. Soc. 2013; 135:4978–4981. [PubMed: 23506476] h Zhang X-D, Wu D, Shen X, Liu P-X, Fan F-Y, Fan S-J. Biomaterials. 2012; 33:4628–4638. [PubMed: 22459191]
6. a Lux F, Mignot A, Mowat P, Louis C, Dufort S, Bernhard C, Denat F, Boschetti F, Brunet C, Antoine R, Dugourd P, Laurent S, Elst LV, Muller R, Sancey L, Josserand V, Coll J-L, Stupar V, Barbier E, Rémy C, Broisat A, Ghezzi C, Le Duc G, Roux S, Perriat P, Tillement O. Angew. Chem. Int. Ed. 2011; 50:12299–12303.b Jiang W, KimBetty YS, Rutka JT, ChanWarren CW. Nat Nanotechnol. 2008; 3:145–150. [PubMed: 18654486] c Huang X, Zhang F, Zhu L, Choi KY, Guo N, Guo J, Tackett K, Anilkumar P, Liu G, Quan Q, Choi HS, Niu G, Sun Y-P, Lee S, Chen X. ACS Nano. 2013; 7:5684–5693. [PubMed: 23731122] d Tang S, Peng C, Xu J, Du B, Wang Q, Vinluan RD, Yu M, Kim MJ, Zheng J. Angew. Chem. Int. Ed. 2016; 128:16273–16277.
7. Kim, M-k, Jeong, H-J., Kao, C-HK., Yao, Z., Paik, DS., Pie, JE., Kobayashi, H., Waldmann, TA., Carrasquillo, JA., Paik, CH. Nucl. Med. Biol. 2002; 29:139–146. [PubMed: 11823118]
8. Liu F, He X, Chen H, Zhang J, Zhang H, Wang Z. Nat. Commun. 2015; 6:8003. [PubMed: 26245151]
9. Xie J, Liu G, Eden HS, Ai H, Chen X. Acc.Chem. Res. 2011; 44:883–892. [PubMed: 21548618]
10. Huang H, Hernandez R, Geng J, Sun H, Song W, Chen F, Graves SA, Nickles RJ, Cheng C, Cai W, Lovell JF. Biomaterials. 2016; 76:25–32. [PubMed: 26517562]

11. a Zhang Y, Jeon M, Rich LJ, Hong H, Geng J, Zhang Y, Shi S, Barnhart TE, Alexandridis P, Huizinga JD, Seshadri M, Cai W, Kim C, Lovell JF. Nat Nanotechnol. 2014; 9:631–638. [PubMed: 24997526] b Lortie M, Beanlands RSB, Yoshinaga K, Klein R, DaSilva JN, deKemp RA. Eur. J. Nucl. Med. Mol. Imaging. 2007; 34:1765–1774. [PubMed: 17619189]
12. a Chauhan VP, Stylianopoulos T, Martin JD, Popovic Z, Chen O, Kamoun WS, Bawendi MG, Fukumura D, Jain RK. Nat Nanotechnol. 2012; 7:383–388. [PubMed: 22484912] b Cheng L, Yang K, Chen Q, Liu Z. ACS Nano. 2012; 6:5605–5613. [PubMed: 22616847]
13. a Yu M, Zhou J, Du B, Ning X, Authement C, Gandee L, Kapur P, Hsieh J-T, Zheng J. Angew. Chem. Int. Ed. 2016; 55:2787–2791.b Tantawy MN, Jiang R, Wang F, Takahashi K, Peterson TE, Zemel D, Hao C-M, Fujita H, Harris RC, Quarles CC, Takahashi T. BMC Nephrology. 2012; 13:168. [PubMed: 23228112]
14. Penna FJ, Chow JS, Minnillo BJ, Passerotti CC, Barnewolt CE, Treves ST, Fahey FH, Dunning PS, Freilich DA, Retik AB, Nguyen HT. The Journal of Urology. 2011; 185:2405–2413. [PubMed: 21511294]
15. Fiel RJ, Datta-Gupta N, Mark EH, Howard JC. Cancer Res. 1981; 41:3543–3545. [PubMed: 7020932]
16. Cheng L, Shen S, Shi S, Yi Y, Wang X, Song G, Yang K, Liu G, Barnhart TE, Cai W, Liu Z. Adv. Funct. Mater. 2016; 26:2185–2197. [PubMed: 27110230]
17. Yang G, Gong H, Qian X, Tan P, Li Z, Liu T, Liu J, Li Y, Liu Z. Nano Res. 2015; 8:751–764.

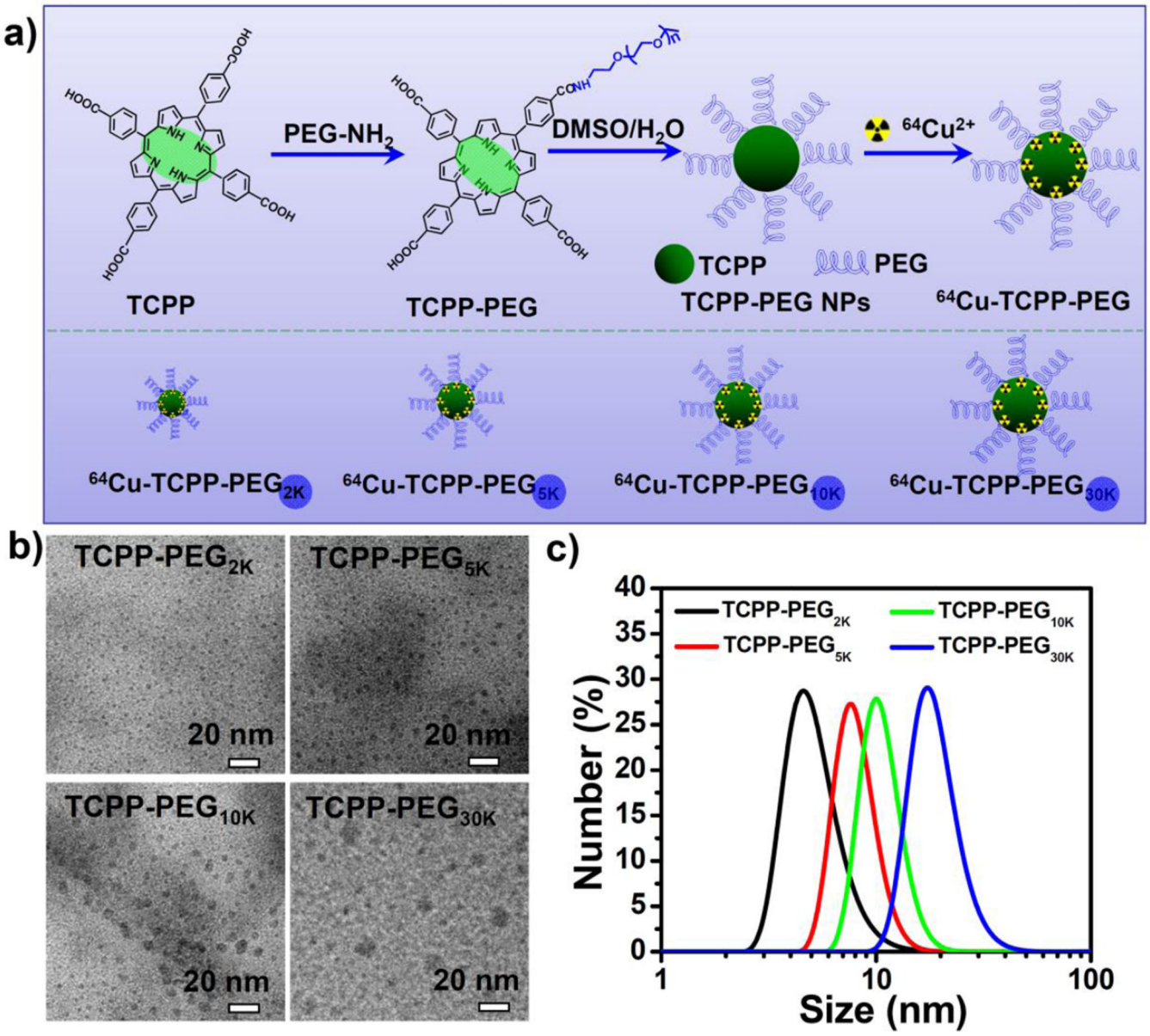

Figure 1.

Synthesis and characterization of TCPP-PEG NPs. **a**) A scheme showing TCPP molecule conjugated with different molecular weight PEG molecules for $^{64}Cu^{2+}$ labeling. **b**) TEM images of TCPP-PEG_{2K}, TCPP-PEG_{5K}, TCPP-PEG_{10K}, and TCPP-PEG_{30K} nanoparticles. **c**) The hydrodynamic diameters (HDs) of TCPP-PEG nanoparticles with various molecule weights after being incubated in water solution. The HDs of the particles were 4.6 ± 1.4 nm for TCPP-PEG_{2K}, 7.5 ± 2.2 nm for TCPP-PEG_{5K}, 10.1 ± 2.8 nm for TCPP-PEG_{10K}, and 17.3 ± 3.2 nm for TCPP-PEG_{30K} nanoparticles.

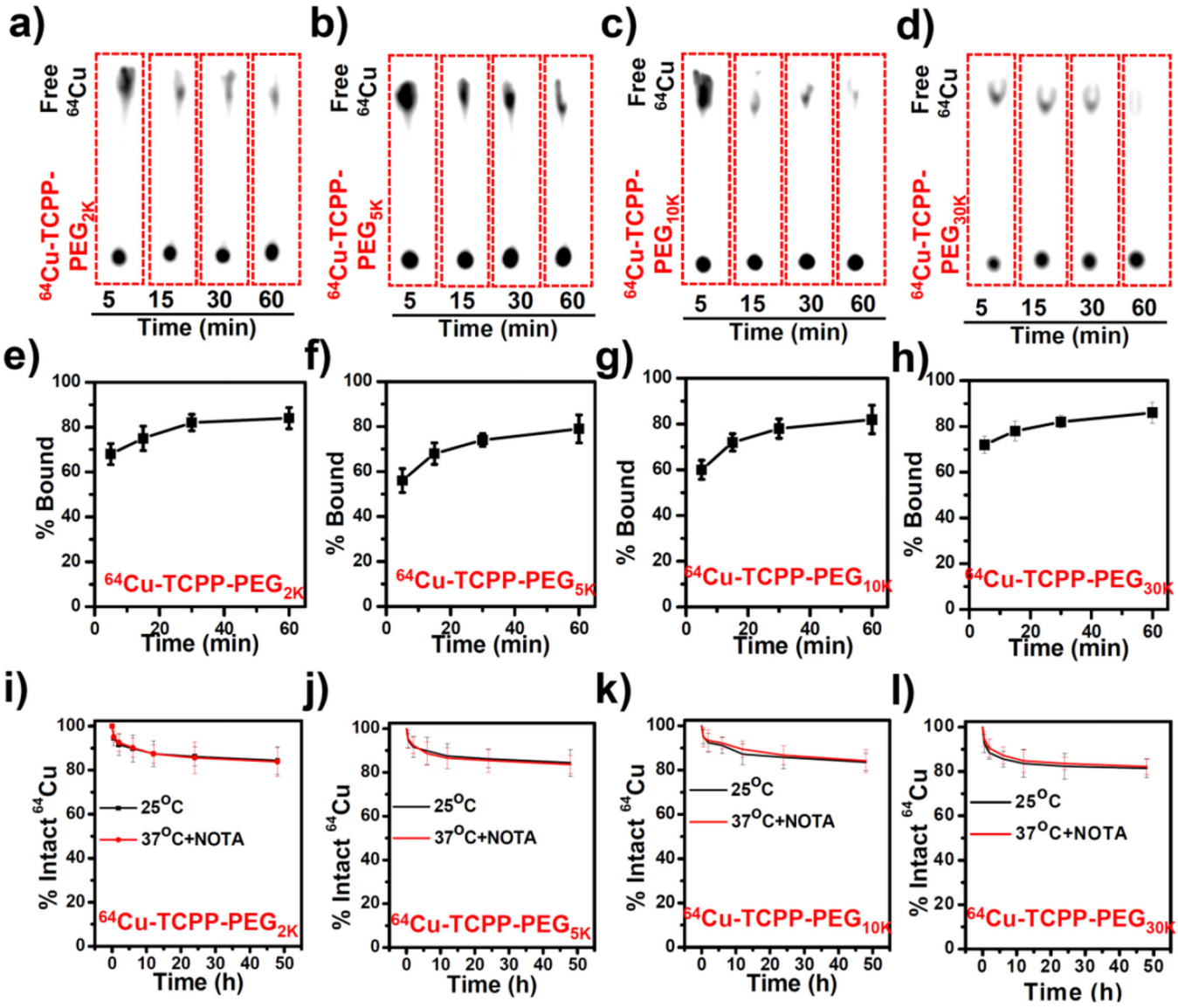

Figure 2.

Intrinsically ^{64}Cu-labeled TCPP-PEG nanoparticles. (**a–d**) Thin-layer chromatography (TLC) plates of TCPP-PEG nanoparticles at various time points after mixing ^{64}Cu with TCPP-PEG nanoparticles: **a**) TCPP-PEG$_{2K}$, **b**) TCPP-PEG$_{5K}$, **c**) TCPP-PEG$_{10K}$, and **d**) TCPP-PEG$_{30K}$. (**e–h**) Quantified labeling yield of ^{64}Cu on TCPP-PEG nanoparticles at various time points after incubation (n = 3): **e**) TCPP-PEG$_{2K}$, **f**) TCPP-PEG$_{5K}$, **g**) TCPP-PEG$_{10K}$, and **h)** TCPP-PEG$_{30K}$.(**i–l**) Stability test of ^{64}Cu labeling on TCPP-PEG nanoparticles after incubation in serum with or without NOTA competitive reaction at 37 °C for different periods of time: **i**) TCPP-PEG$_{2K}$, **j**) TCPP-PEG$_{5K}$, **k**) TCPP-PEG$_{10K}$, and **l**) TCPP-PEG$_{30K}$.

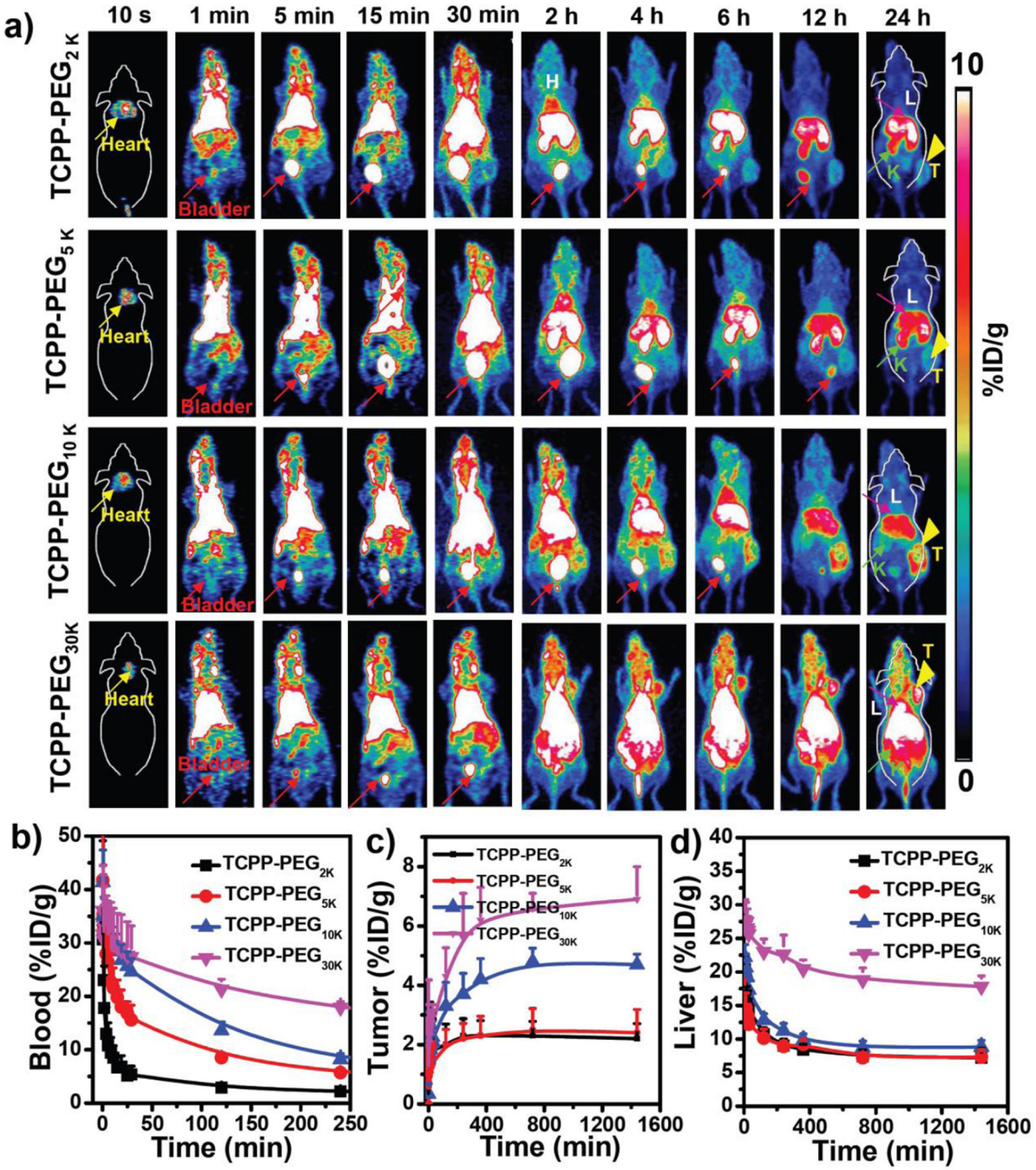

Figure 3.

In vivo PET imaging: **a**) PET images of 4T1 tumor-bearing mice taken at various time points (10 s, 1 min, 5 min, 15 min, 30 min, 2 h, 4 h, 6 h, 12 h, and 24 h) post-injection of ^{64}Cu-TCPP-PEG$_{2K}$, ^{64}Cu-TCPP-PEG$_{5K}$, ^{64}Cu-TCPP-PEG$_{10K}$, and ^{64}Cu-TCPP-PEG$_{30K}$ nanoparticles. Liver (L), Kidneys (**K**), Heart, and Bladder are indicated in each figure. Tumor (T) is indicated by yellow arrowheads. (**b–d**) Time-activity curves of ^{64}Cu-TCPP-PEG (2K, 5K, 10K, and 30K) in different major organs of (**b**) blood, (**c**) tumor, and (**d**) liver.

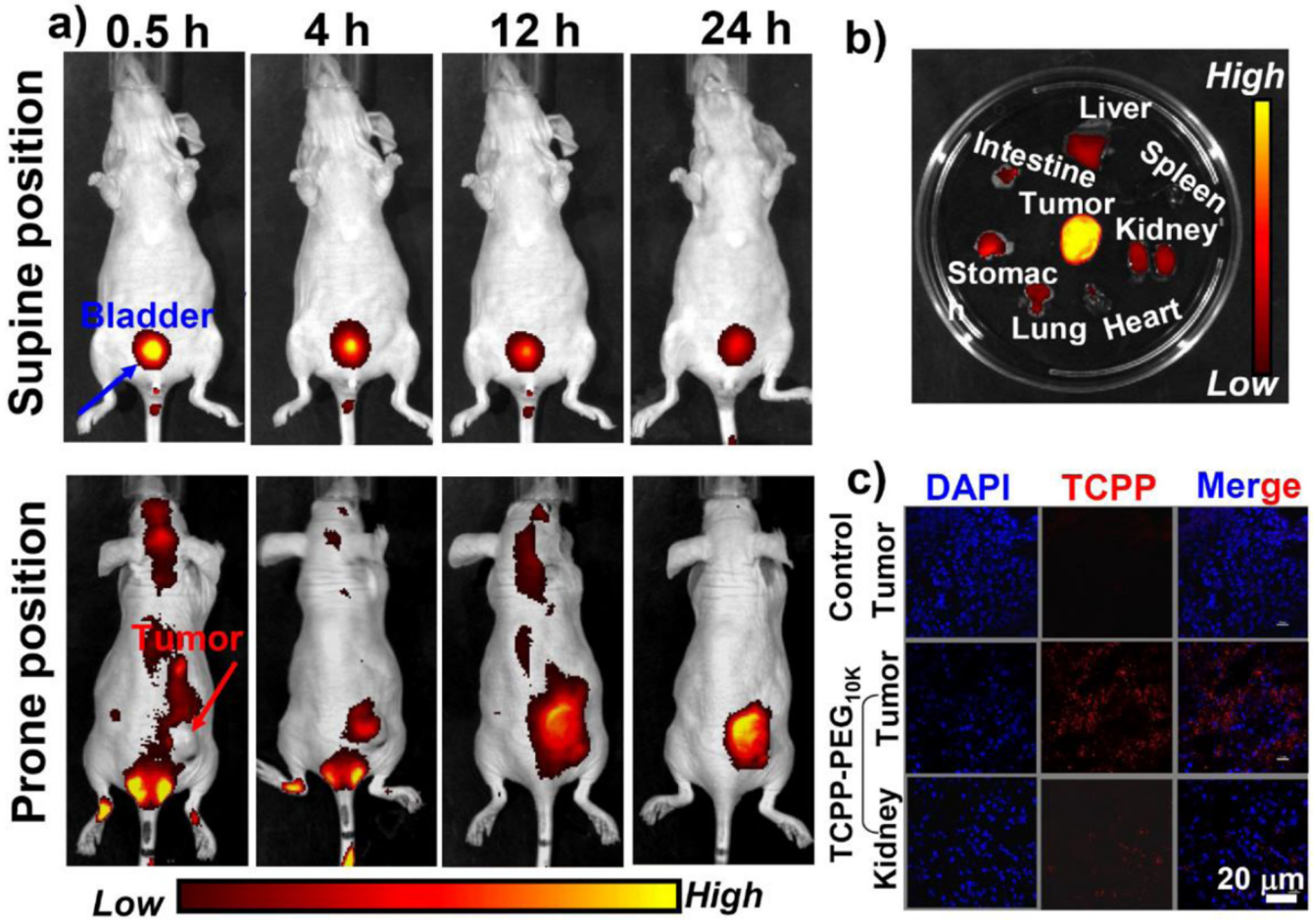

Figure 4.

In vivo and *ex vivo* fluorescence imaging: **a&b**) *In vivo* fluorescence images of 4T1 tumor-bearing nude mice taken at different time points post-injection of TCPP-PEG_{10K} nanoparticles with prone (**top**) and supine (**bottom**). **b**) *Ex vivo* fluorescence images of major organs and tumor dissected from mice injected with TCPP-PEG_{10K} nanoparticles at 24 h p. i.. (**c**) Confocal images of tumor and kidney tissues after i. v. injection TCPP-PEG_{10K} nanoparticles or not at 24 h p. i.. Red color represents the fluorescence signal from TCPP molecule.

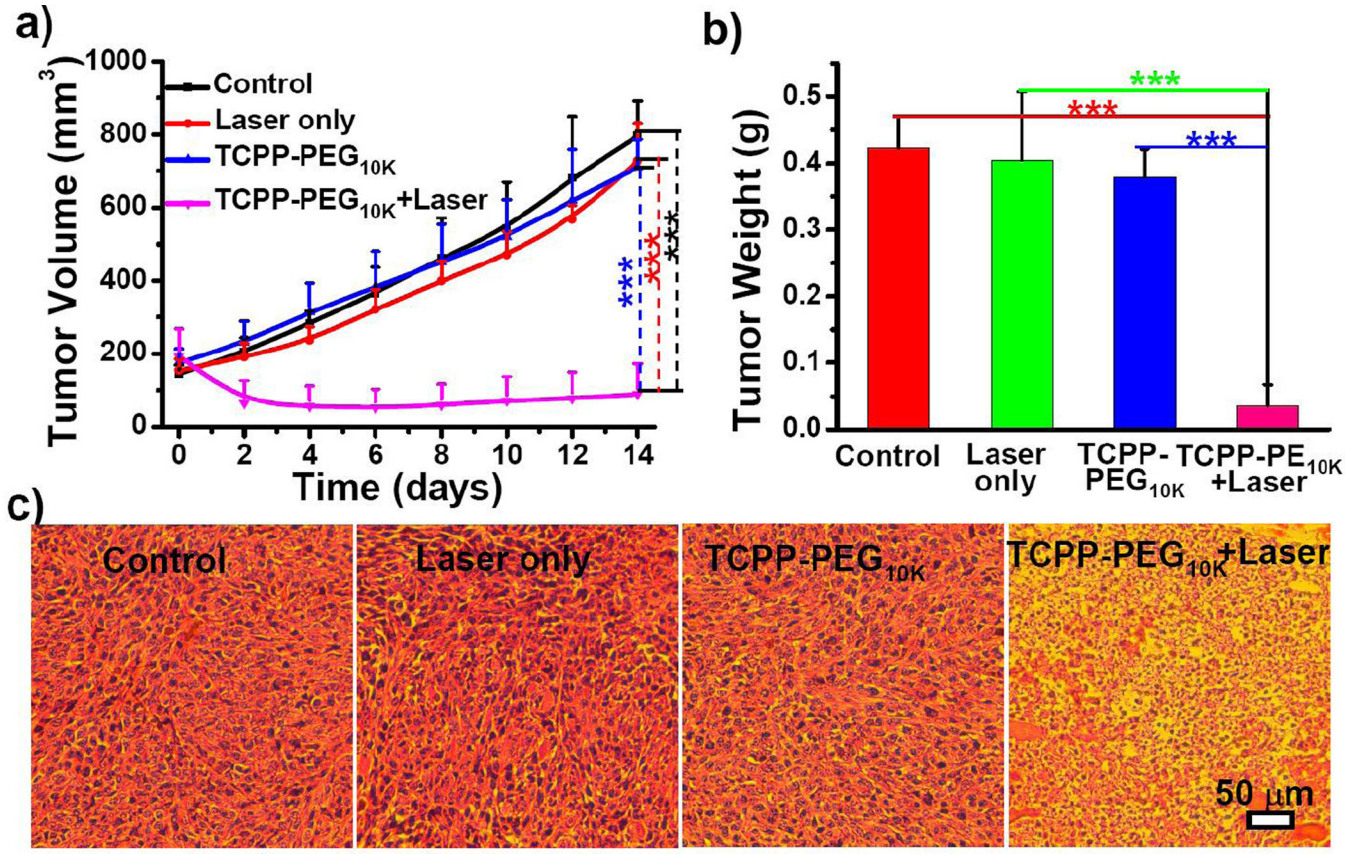

Figure 5.

In vivo PDT. **a**) Tumor growth curves of different groups of mice after various treatments indicated. For the treatment group, four mice injected with TCPP-PEG_{10K} nanoparticles at 24 h p. i. were exposed to the 658-nm laser (50 mW/cm^2, 30 min). Other three groups of mice were used as controls: untreated (Control, n =4); laser only without TCPP-PEG_{10K} injection (Laser only, n =4); TCPP-PEG_{10K} nanoparticles injected but without laser irradiation (TCPP-PEG_{10K}, n = 4. Error bars were based on SD. **b**) Tumor weight of different groups taken at the 14^{th} day. **c**) H&E stained tumor slices collected from different groups of mice on the following day after various treatments. Statistical analysis was performed using the student's two-tailed t test: *$p < 0.05$, **$p < 0.01$, and ***$p < 0.001$.